Formation of Iron Oxides by Surface Oxidation of Iron Plate[†]

Marijan Marciuš, Mira Ristić,* Mile Ivanda, and Svetozar Musić

Ruđer Bošković Institute, P. O. Box 180, HR-10002 Zagreb, Croatia

Abstract. Oxidation of iron plates (α-phase) at high temperatures and in atmospheric conditions was monitored. The composition of oxidation products was analyzed with XRD, Raman and Mössbauer spectroscopies, whereas the morphologies of oxidation products were inspected by FE-SEM. The oxidation products formed at 300 and 400 °C consisted dominantly of magnetite and small fractions of hematite, whereas at 500 and 600 °C hematite was the dominant phase, as shown by XRD. In all these samples Raman spectra showed the presence of hematite in the outer oxidation layer. FE-SEM analysis showed the formation of nanowires at 500 °C and vertically grown hematite spikes against the lower oxidation layers at 600 °C. Oxidation products formed at 800 °C consisted of wüstite ($Fe_{1-x}O$) as the dominant phase, nonstoichiometric magnetite ($Fe_{3-x}O_4$) and hematite ($α-Fe_2O_3$) in small fractions. The surface of these oxidation layers showed a hierarchical microstructure, as well as the hexagonal hematite rods vertically grown against the lower oxidation layers. The formation of the oxidation products can be considered a process which includes the oxidation of α-Fe to $Fe_{1-x}O$ and its transformation to $Fe_{3-x}O_4$ that further transforms to $α-Fe_2O_3$, probably *via* a short-lived $γ-Fe_2O_3$ (maghemite) phase. (doi: 10.5562/cca1943)

Keywords: corrosion, α-Fe, hematite, magnetite, wüstite

INTRODUCTION

Iron oxides are typical products of iron (steel) oxidation at high temperatures. The type of atmosphere, the presence of alloying elements and the chemical pretreatment of surfaces influence the phase composition and microstructure of the formed surface layers. The investigation of iron (steel) at high temperatures is important from both the academic and technological standpoints. This investigation may provide information about how oxidation proceeds on the iron (steel) surface and what can be expected in the behavior of this material in real applications under similar conditions. The oxide layers on iron (steel) surfaces are not easy to analyze due to their complex phase composition, nonstoichiometry and/or very small particles. For that reason different experimental techniques are needed for the characterization of the oxide layers formed on the surface of iron (steel).

Bredesen and Kofstad investigated[1,2] reaction kinetics and development of scale morphology during the oxidation of γ-Fe in CO_2-CO atmosphere. Wüstite was the initially formed oxidation product. The chemical state of iron on the surface of carburized steel was analyzed by CEMS (Conversion Electron Mössbauer spectroscopy). The absence of iron carbide was found in the surface layer of the carburized and annealed steel.[3] Lee and Choi[4] investigated the high temperature oxidation of steel between 1100 and 1250 °C for up to 2 h at 1 atm pressure of air or gas mixture 85 % N_2 – 10 % CO_2 – 5 % O_2. The oxidation process followed the initial linear rate law, then gradually transformed to a nearly parabolic rate law. In addition to Fe_3O_4, Fe_2O_3 and FeO oxides in rust the alloying elements such as Mn, P, S, Si and Ti were found as well. Sato and Young[5] investigated the corrosion of iron at 900 °C in atmospheres containing HCl and H_2O vapors. The authors observed FeO, Fe_3O_4 and Fe_2O_3 in three layers as corrosion products. HCl and O_2 represent a very corrosive atmosphere for iron, which, for example, can jeopardize the design life of incineration plants. Guillamet *et al.*[6] and Nomura and Ujihira[7] investigated the corrosion products of chemically treated AISI 304 and 316 (SUS304 and SUS316) steels heated at high temperatures.

Simmons *et al.*[8] investigated the oxidation of electroplated iron at 225, 350, and 450 °C using CEMS. Nonstoichiometric magnetite ($Fe_{3-x}O_4$) and mixture of stoichiometric magnetite and hematite were formed upon iron oxidation at 350 °C for short times, whereas near stoichiometric magnetite was only the oxide phase formed upon iron oxidation at 450 °C. Ohashi *et al.*[9]
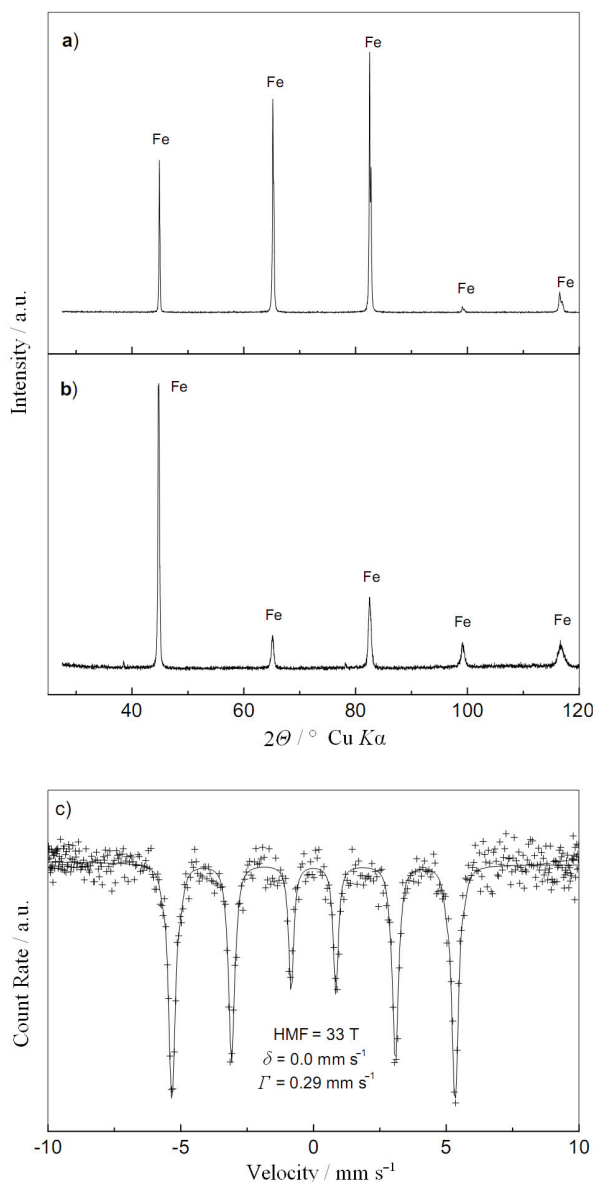
Figure 1. XRD patterns of (a) iron plate as supplied, (b) iron plate cut into small splinters corresponding to α-phase, and (c) ^{57}Fe Mössbauer spectrum also showing the presence of α-Fe.

oxidized iron foil (99.9 % Fe) in oxygen atmosphere at 680 torr between 300 and 600 °C. At temperatures higher than 400 °C magnetite and hematite were the oxidation products. No change in the Mössbauer spectrum by heating the iron foil at 300 °C for 20 days was found. Huffman and Podgurski[10,11] oxidized ^{57}Fe enriched iron in pure oxygen at 150 to 500 °C and the oxidation products were examined by Electron Re-emission Mössbauer (ERM) spectroscopy. Magnetite and hematite were detected and with this technique the thickness of oxide layers between ≈ 2 and 300 nm could be estimated. The applications of Mössbauer spectroscopy in corrosion studies were reviewed in reference literature.[12–14]

Ohtsuka *et al.*[15] used Raman spectroscopy to analyze thin corrosion films formed on the iron surface between 100 and 150 °C. It was found that in dry air magnetite is the dominant phase, whereas in the presence of water vapor in air the formation of hematite is accelerated. Aligned hematite nanowires were obtained[16] by iron oxidation between 540 and 600 °C in a flow gas mixture consisting of 19.3 % CO_2, 0.14 % SO_2 and 80.56 % NO_2 and containing some H_2O vapor produced by purified water. Hematite wires with diameters between 20 and 40 nm and lengths 2 to 5 μm were found. Candron and Buscail[17] used *in situ* high temperature XRD to investigate the oxidation of yttrium implanted in extra low carbon steel and pure iron. The yttrium implantation promoted the formation of protective oxides to corrosion, $FeYO_3$ and Fe_2YO_4.

Environmental SEM was used[18] in *in situ* investigation of the influence of H_2O on iron oxidation at 500 °C. In dry and wet air two magnetite forms beneath a thin fine-grained hematite layer were obtained, whereas only a two-layered magnetite formed in the presence of H_2O. In the presence of a low level of water vapor a thicker hematite layer in the form of whiskers was formed. It was concluded that the surface of metal grains, the thickness of hematite layers, the oxide grain size and the environment are the factors likely to influence the oxidation of iron.

This brief introduction shows the complexity of the oxidation process on the surface of iron (steel). In many cases a limited number of samples and parameters have been taken into account, and the morphological investigations of oxidation products have been particularly scant. In the present work we used a simple system as a model: the iron (α-phase) plate and its oxidation in air atmosphere at high temperatures. The grown oxidation layers were characterized with XRD, Raman and Mössbauer spectroscopies, as well as FE-SEM coupled with EDS.

EXPERIMENTAL

Iron sheets (99.8 % purity) 1 mm thick were supplied by NEWMET Koch, U.K., and used as received. They were cut into smaller plates, cleaned with acetone, then heated in the laboratory furnace in air atmosphere at predetermined temperatures and times. The selected samples were analyzed using the following instrumentation:

X-ray diffraction (XRD) patterns were recorded at 20 °C using an APD 2000 X-ray powder diffractometer with Cu$K\alpha$ (λ = 1.54059 Å) radiation (conditions: 40 kV and 30 mA), manufactured by *ItalStructures*.

The Raman spectra were recorded using a *Horiba-Jobin Yvon T64000* Raman spectrometer. The 514.5 nm argon laser beam was used as the excitation source.
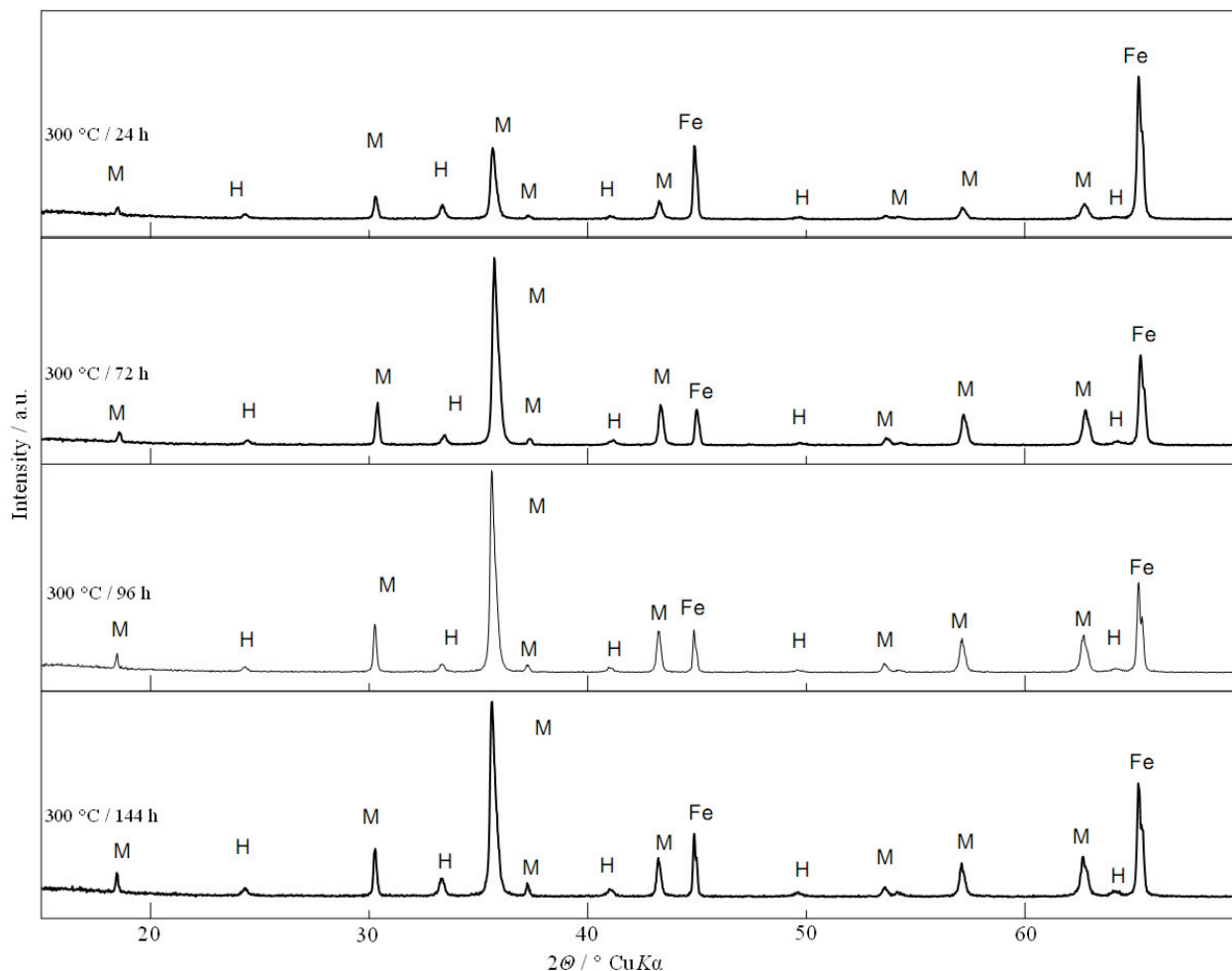
Figure 2. XRD patterns of oxide layers formed on the iron plate at 300 °C between 24 and 144 h. Key: M = magnetite, H = hematite and Fe = iron plate.

A Mössbauer spectrometer built in *WissEl* configuration was used. ^{57}Co in a rhodium matrix was used as the Mössbauer source. The velocity scale and all the data refer to the α-Fe absorber at 20 °C. The deconvolution of the Mössbauer spectrum was performed using the *MossWin* computer program.

The samples were also examined using a thermal field emission scanning electron microscope (FE-SEM, model JSM-7000F) manufactured by JEOL Ltd. An energy dispersive X-ray spectrometer, EDS/INCA 350, manufactured by Oxford Instruments, was coupled with FE-SEM and used to determine the chemical composition of the samples examined.

RESULTS AND DISCUSSION

Figure 1 shows XRD patterns of (a) the iron plate as supplied, and (b) fine grained iron plate cuttings. These XRD patterns correspond to an α-Fe phase and the differences in relative line intensities are due to the preferential orientation effect. The α-Fe phase is also con-

firmed by the Mössbauer spectrum shown in Figure 1c. Figure 2 shows an XRD patterns of the oxide layers formed on the iron plate at 300 °C between 24 and 144 h. The main crystalline phase corresponds to magnetite (M), while hematite (H) is present as a minor crystalline phase. XRD patterns also show an increase in the relative intensity of magnetite lines with prolonged corrosion time. At the same time, the relative intensity of the substrate lines (α-Fe) decreased, thus indicating an increase in thickness of oxide products. Figure 3 shows XRD patterns of the oxide layer produced upon heating of the iron plate at 400, 500 and 600 °C for 96 h. XRD pattern of the oxide layer formed at 400 °C showed that the most intensive diffraction line was M(311) corresponding to magnetite. The oxide layer formed at 500 °C showed a significant increase of the H(300) diffraction line corresponding to hematite, whereas the oxide layer formed at 600 °C showed an almost diminishing diffraction line M(311) and a strong increase in the intensity of the diffraction line H(300). This result can be explained by the preferential crystal growth of hematite in the oxidation layer formed at 600 °C.
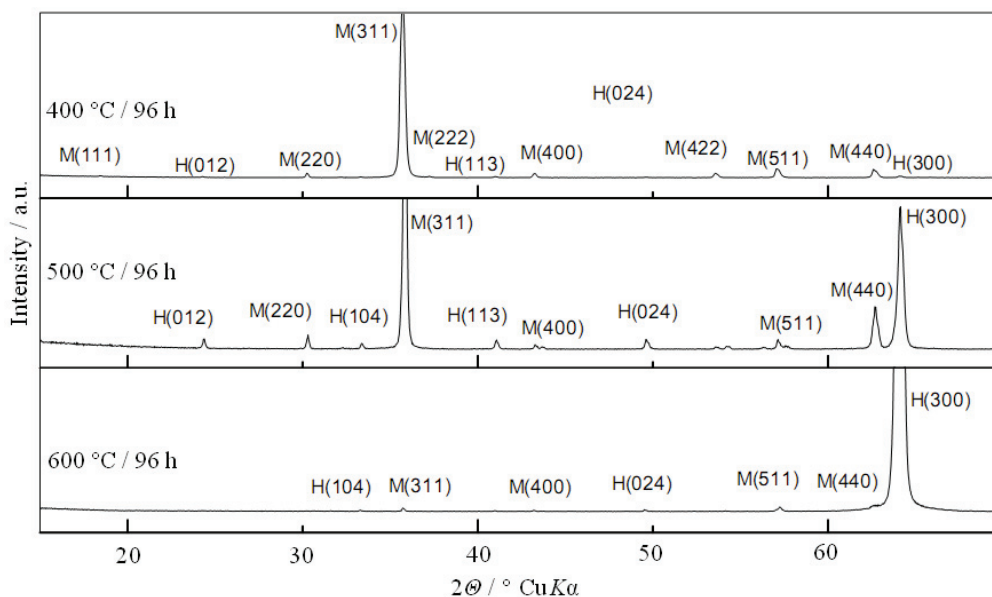
Figure 3. XRD patterns of oxide layers formed on the iron plate at 400, 500 and 600 °C for 96 h: Key: M = magnetite, H = hematite.

Raman spectroscopy is a very useful technique in the surface analysis of many materials. Figure 4 shows Raman spectra on the surface of oxidation layers formed at 300, 400 and 500 °C for 24 h. These spectra can be assigned to hematite according to Raman bands at 227 (A_{1g}), 247(E_g), 293(E_g), 301(E_g), 414(E_g), 499(A_{1g}), 614(E_g) and 661
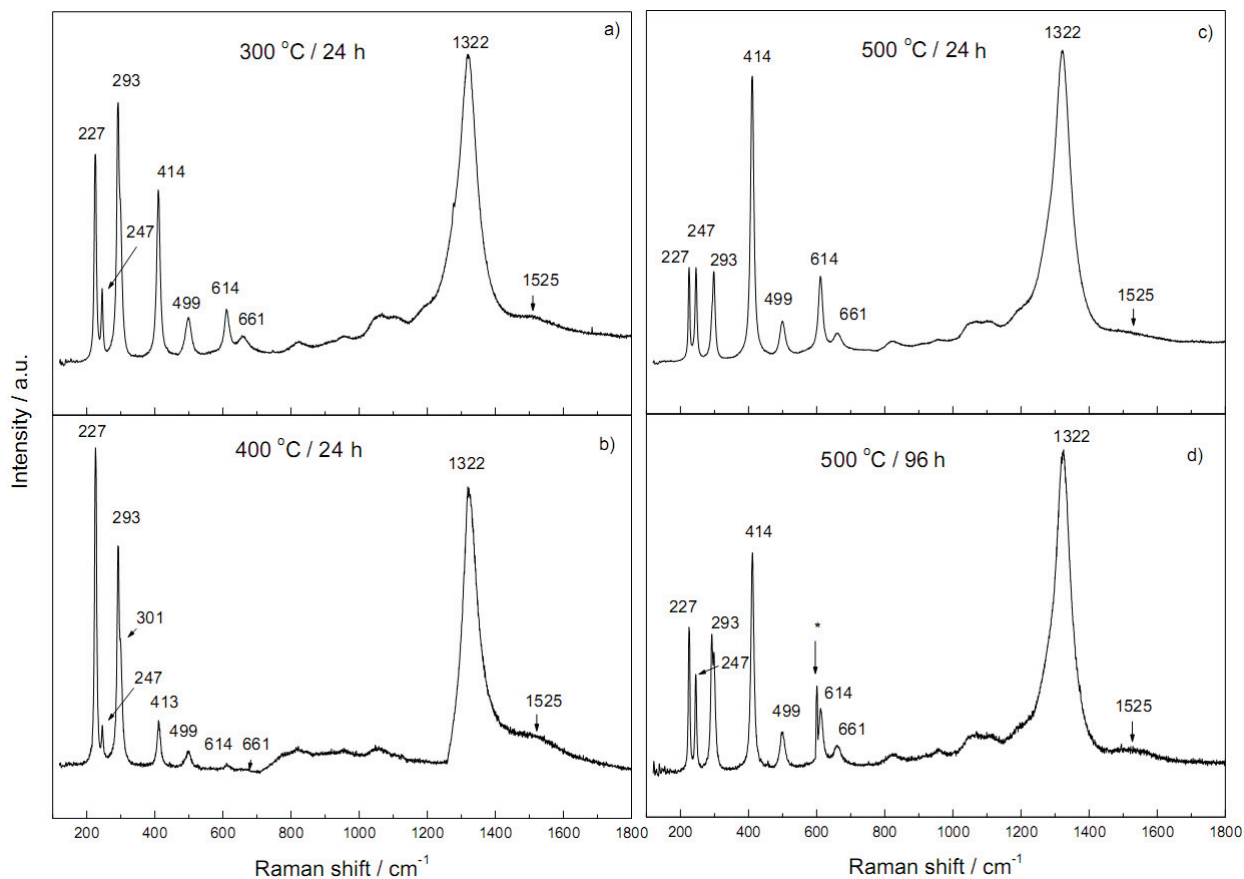

Figure 4. Raman spectra of oxide layers on the iron plate formed (a) at 300 °C for 24 h, (b) at 400 °C for 24 h, (c) at 500 °C for 24 h, and (d) at 500 °C for 96 h.
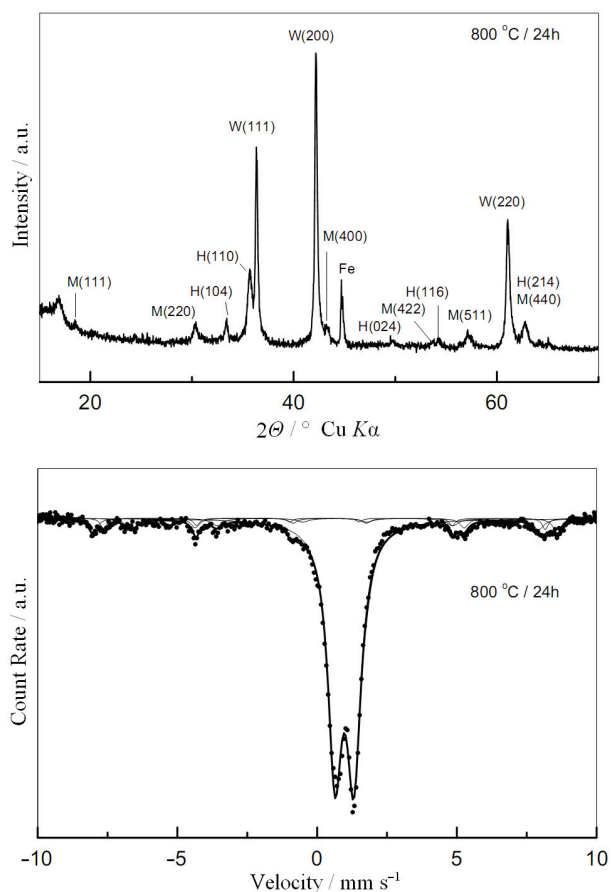
Figure 5. XRD pattern (upper) and ^{57}Fe Mössbauer spectrum (down) of the scraped oxide layer formed at 800 °C for 24 h. Key: W = wüstite; M = magnetite; H = hematite.
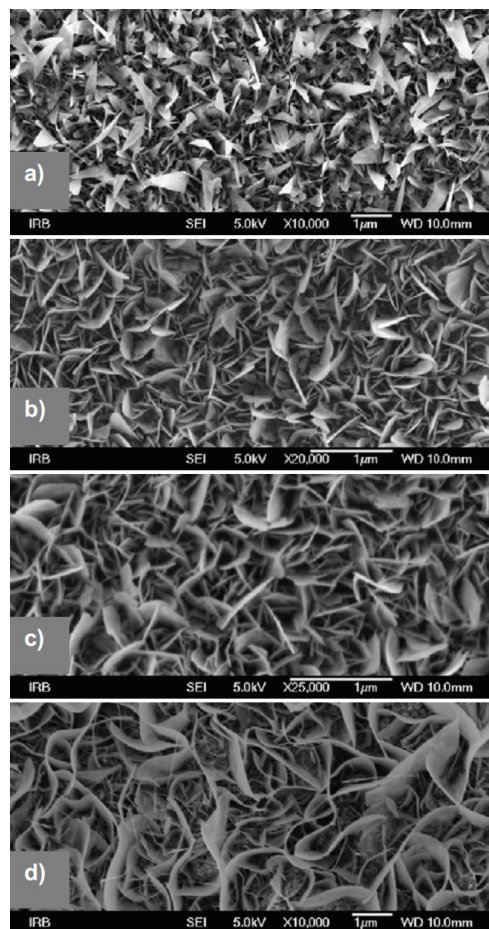
Figure 6. FE-SEM images of the surfaces upon iron plate oxidation at (a) 300 °C for 96 h, (b) 400 °C for 24 h, (c) 400 °C for 96 h, and (d) 500 °C for 24 h.

(LO E_u). These Raman spectra also show a very strong and broad band at 1322 cm^{-1} as well as a very broad band of relatively weak intensity at 1525 cm^{-1}. McCarty[19] assumed that the band at ≈ 1320 cm^{-1} was an overtone associated with a Raman-forbidden longitudinal-optical (LO) phonon near 660 cm^{-1}, and not due to magnetic scattering. Massey *et al.*[20] identified the two-magnon scattering as a weak and broad band at ≈ 1525 cm^{-1}, showing a temperature dependence consistent with a magnetic origin. The shape and location of Raman bands depend on particle size, as shown in the example of zinc oxide.[21] Likewise, it was found that the profile of the Raman

spectrum of hematite strongly depends on the excitation radiation lines of the laser beam.[22] In the Raman spectra shown in Figure 4, the characteristic bands T_{2g} and A_{1g} corresponding to magnetite[23,24] are not visible. A significant discrepancy between XRD and Raman spectrum analyses of the same sample may be explained by the fact that X-ray beams penetrate much deeper under the surface of the sample, whereas Raman spectroscopy is a truly surface-specific analysis technique. Raman spectra in Figure 4 showed significant changes in the relative intensities of certain bands. For example, the relative

Table 1. Mössbauer parameters calculated for scraped layer formed on iron plate upon heating for 24 h at 800 °C

Line	δ_{Fe} / mm s^{-1}	Δ or Eq / mm s^{-1}	HMF / T	Γ / mm s^{-1}	Area / %	Identification
Q	0.99	0.67		0.53	74	wüstite
M1	0.37	−0.22	51.4	0.63	10	hematite
M2	0.67	0.04	45.5	0.58	10	magnetite
M3	0.27	0.01	48.8	0.49	6	magnetite

Key: δ = isomer shift relative to α-Fe at RT; B_{hf} = hyperfine magnetic field.
Δ or Eq = quadrupole splitting; Γ = line-width.
Errors: δ = ± 0.01 mm s^{-1}; Δ or Eq = ± 0.01 mm s^{-1}; B_{hf} = ± 0.2 T

Element	Atomic / %
O	4,24
Fe	95,76
Totals	100

(A)

Element	Atomic / %
O	58,29
Fe	41,71
Totals	100

(B)

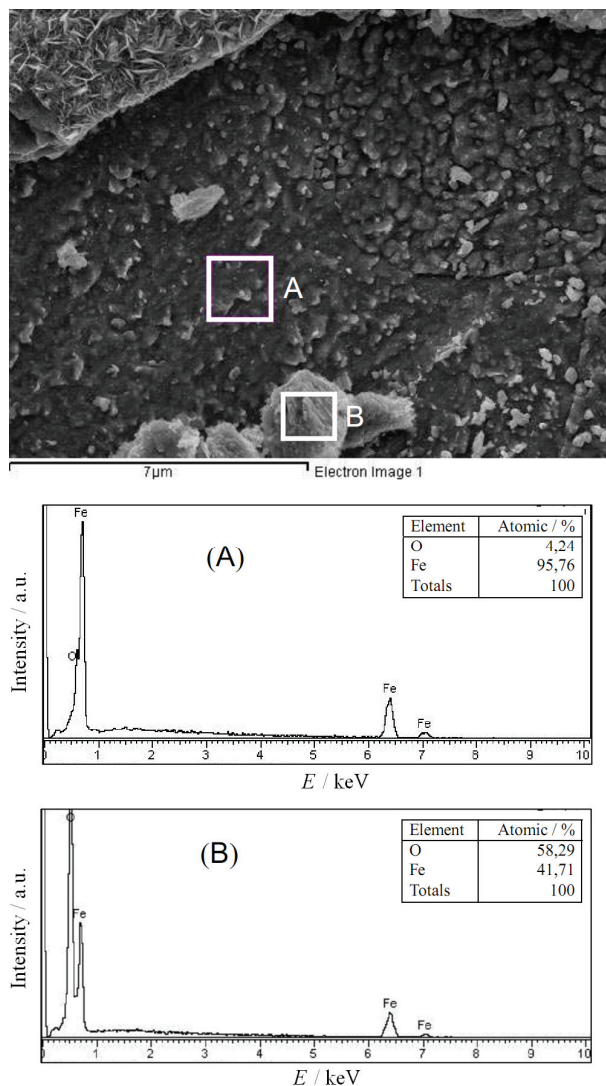**Figure 7.** EDS analysis of (A) adherent and (B) non-adherent layer of oxide layer obtained upon heating at 400 °C for 96 h.
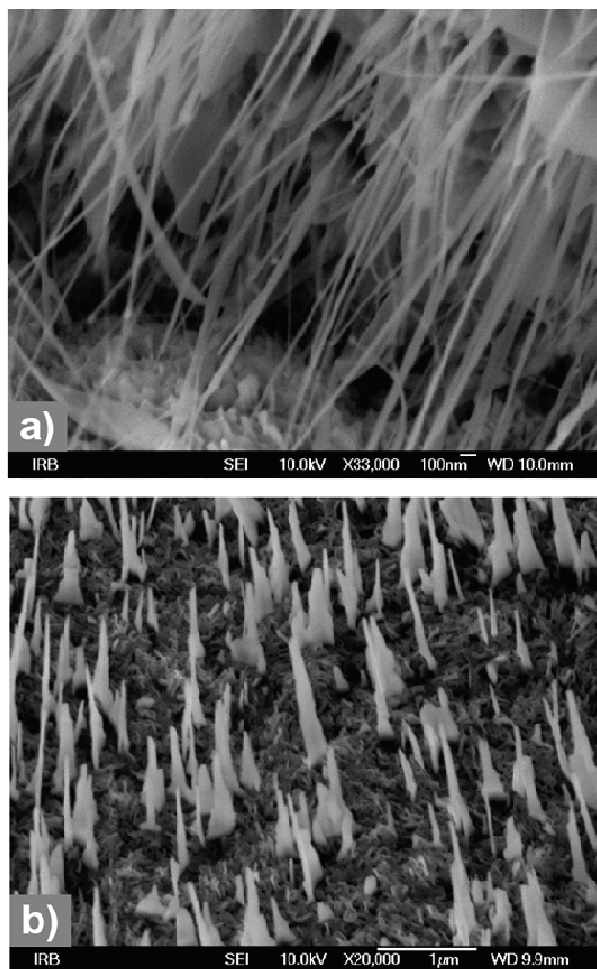

Figure 8. Preferential crystal growth of hematite on the iron plate upon heating (a) at 500 °C for 96 h, and (b) at 600 °C for 96 h.

intensities of the bands at 227 and 293 cm^{-1} are significantly decreased, whereas the relative intensities of the bands 247 and 414 cm^{-1} are increased. This effect can be related to the preferential crystal growth of hematite during the high-temperature oxidation of iron.

The XRD pattern (20 °C) and the Mössbauer spectrum (20 °C) of the scraped oxide layer formed at 800 °C for 24 h are shown in Figure 5. XRD lines of wüstite were dominant in intensity. XRD lines corresponding to magnetite and hematite showed the presence of these phases in small fractions. This was also confirmed by the Mössbauer spectrum. The Mössbauer spectrum is resolved taking into account the superposition of one central quadrupole doublet and three magnetic splitting components. Calculated Mössbauer parameters are given in Table 1. The central quadrupole doublet, Q, corresponds to wüstite (Fe$_{1-x}$O), the magnetic splitting component M1 corresponds to hematite (α-Fe$_2$O$_3$) and

the magnetic splitting components M2 and M3 correspond to nonstoichiometric magnetite (Fe$_{3-x}$O$_4$).

Different morphologies of oxidation products of iron in dependence on temperature and time were observed. The representative results obtained by FE-SEM are shown in Figures 6 to 9. Figure 6a shows the surface of oxidized iron for 96 h at 300 °C. Hematite particles are elongated and very thin (nanometric size) suggesting the shape of corn plant leaves. With an increase in heating temperature up to 400 °C the particles increased in size perpendicular to their elongation, but they remained thin, and that increase was more pronounced upon heating of iron at 500 °C (Figures 6bcd). Figure 7 shows EDS analysis after a non-adherent oxide layer, obtained upon heating for 96 h at 400 °C, was removed. EDS analysis of the area **A** showed the dominant fraction of iron due to the vicinity of metallic iron and a small fraction of oxygen. The presence of oxygen may be due to a small amount of Fe$_{1-x}$O and Fe$_{3-x}$O$_4$. An analysis of area **B** showed the atomic ratio of Fe to O close to hematite. Hematite nanowires were produced upon heating of the iron plate for 96 h at 500 °C (Figure 8a). They
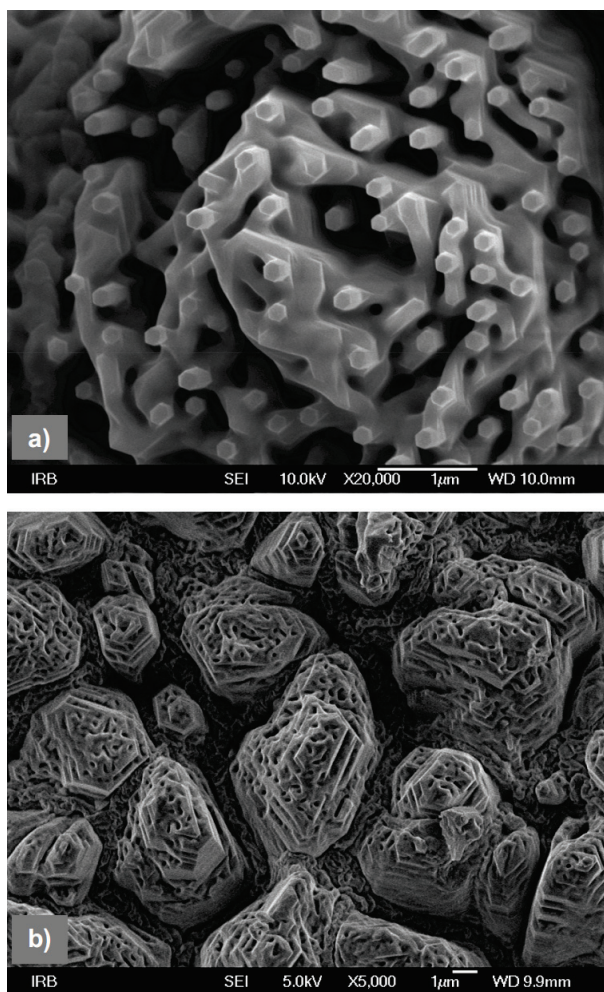
Figure 9. FE-SEM images of oxide layers formed on the iron plate at 800 °C for 24 h showing (a) hexagonal rods of hematite crystallized perpendicular to the substrate, and (b) development of a hierarchical microstructure.

were produced by the recrystallization process in one direction of crystal growth. The surface growth of hematite in one direction is well visible upon heating of iron plate for 96 h at 600 °C (Figure 8b). These results can be related to the previous conclusions based on the XRD and Raman measurements. Finally, the oxide layer morphologies obtained upon heating of the iron plate for 24 h at 800 °C are shown in Figure 9. Figure 9a shows the crystal growth of hexagonal rods of hematite perpendicular to the substrate, whereas the formation of a hierarchical microstructure is shown in Figure 9b.

CONCLUSION

Magnetite and hematite were the oxidation products on the iron plate (α-phase) between 300 and 600 °C according to XRD analysis. On the basis of XRD patterns of samples prepared at 500 to 600 °C the preferential crys-

tal growth of hematite in the outer layer is suggested. Raman spectroscopy as a typical surface technique showed only the presence of hematite. The relative intensities of Raman bands corresponding to hematite differed for samples prepared at 300 and 400 °C, and those prepared at 500 and 600 °C. XRD and Mössbauer spectroscopy of the oxide layer formed on the iron plate at 800 °C for 24 h showed the presence of wüstite as a dominant phase, and magnetite and hematite as small fractions. The iron plate oxidation at high temperatures in air atmosphere starts with the formation of wüstite (generally, $Fe_{1-x}O$) which transforms to nonstoichiometric magnetite. The nonstoichiometry of magnetite may also vary in dependence on the depth of the oxide layer. On the outer surface there is solid state transformation of magnetite to hematite probably *via* a short-lived maghemite phase. FE-SEM of samples prepared at 300 to 400 °C showed very thin hematite particles in the form of plant leaves, whereas the samples prepared at 500 and 600 °C for 96 h showed a highly oriented crystal growth of hematite in one direction. Upon oxidation of the iron plate at 800 °C for 24 h, the hierarchical microstructure and growth of hexagonal hematite rods grown vertically against the lower oxidation layers were observed.

REFERENCES

1. R. Bredesen and P. Kofstad, *Oxid. Met.* **34** (1990) 361–379.
2. R. Bredesen and P. Kofstad, *Oxid. Met.* **35** (1991) 107–137.
3. A. Handa, Y. Ujihira, and I. Okabe, *J. Mater. Sci.* **16** (1981) 1999–2002.
4. D. B. Lee and J. W. Choi, *Oxid. Met.* **64** (2005) 319–329.
5. Y. Sato and D. J. Young, *Oxid. Met.* **55** (2001) 243–260.
6. R. Guillamet, M. Lenglet, L. Gazin, B. Hannoyer, and J. Lopitaux, *Surf. Interface Anal.* **20** (1993) 15–20.
7. K. Nomura and Y. Ujihira, *J. Mater. Sci.* **25** (1990) 1745–1750.
8. G. W. Simmons, E. Kellerman, and H. Leidheiser, Jr., *Corrosion* **29** (1973) 227–233.
9. H. Ohashi, M. Koizumi, and T. Morozumi, *Bull. Fac. Eng., Hokkaido Univ. No.* **72** (1974) 145–153.
10. G. P. Huffman and H. H. Podgurski, *Oxid. Met.* **10** (1976) 377–401.
11. G. P. Huffman and H. H. Podgurski, *Oxid. Met.* **15** (1981) 323–329.
12. F. J. Berry, M. E. Brett, P. Bowen, and W. Jones, *J. C. S. Dalton* (1981) 1450–1455.
13. A. Vértes and I. Czakó-Nagy, *Electrochim. Acta* **34** (1989) 721–758.
14. Y. Ujihira and K. Nomura, *Analyses of Corrosion Products of Steel by Conversion Electron Mössbauer Spectroscopy*, Signpost, 1996.
15. T. Ohtsuka, K. Kubo, and N. Sato, *Corrosion-NACE* **42** (1986) 476–481.
16. Y. Y. Fu, R.M. Wang, J. Xu, J. Chen, Y. Yan, A.V. Narlikar, and H. Zhang, *Chem. Phys. Lett.* **379** (2003) 373–379.
17. E. Caudron, H. Buscail, *Mater. Chem. Phys.* **64** (2000) 29–36.
18. F. Jonsson, B. Pujilaksono, S. Hallström, J. Ågren, J.-E. Svensson, L.-G. Johansson, and M. Halvarsson, *Corrosion Sci.* **51** (2009) 1914–1924.
19. K. F. McCarty, *Solid State Commun.* **68** (1998) 799–802.
20. M. J. Massey, U. Baier, R. Merlin, and W. H. Weber, *Phys. Rev. B* **41** (1990) 7822–7827.
21. M. Ristić, S. Musić, M. Ivanda, and S. Popović, *J. Alloys Comp.*

397 (2005) L1-L4.

22. J. Wang, W. B. White, and J. H. Adair, *J. Am. Ceram. Soc.* **88** (2005) 3449–3454.

23. I. Chamritski and G. Burns, *J. Phys. Chem. B* **109** (2005) 4965–4968.

24. M. Baghaie Yazdi, M.-L. Goyallon, T. Bitsch, A. Kastner, M. Schlott, and L. Alff, *Thin Solids Films* **519** (2011) 2531–2533.